

Active RIS vs. Passive RIS: Which Will Prevail in 6G?

Zijian Zhang, Linglong Dai, Xibi Chen, Changhao Liu, Fan Yang, Robert Schober, and H. Vincent Poor

Abstract—From 1G to 5G, wireless channels have been traditionally considered to be uncontrollable. Thanks to the recent advances in meta-materials, reconfigurable intelligent surfaces (RISs) have emerged as a new paradigm for controlling wireless channels intelligently, thus making it a revolutionary technique for future 6G wireless communications. However, due to the “double fading” effect, RIS only achieves a negligible capacity gain in typical communication scenarios, which however has been widely ignored in many existing works. In this paper, the concept of active RIS is proposed to break this fundamental physical limit. Different from the existing passive RIS that reflects signals passively without amplification, active RIS can actively amplify the reflected signals. We then develop a signal model for active RIS, which is validated through experimental measurements. Based on this new signal model, we analyze the capacity gain achievable by active RIS and formulate the capacity maximization problem in an active RIS aided system. Next, a joint transmit and reflect precoding algorithm is proposed to solve this problem. Finally, extensive results show that, compared with the baseline without RIS, the existing passive RIS can realize a negligible capacity gain of only 3% in typical application scenarios, while the proposed active RIS can achieve a noticeable capacity gain of 129%, thus overcoming the fundamental limit of “double fading” effect.

I. INTRODUCTION

Over the past few decades, wireless communications have provided society with significant benefits. From 1G to 5G, the system capacity has been significantly improved by advancing the transceiver design, while the wireless channels have been usually considered to be uncontrollable. Recently, with the interdisciplinary development of meta-materials, electromagnetics, and wireless communications, a revolutionary technique called reconfigurable intelligent surface (RIS) has been proposed [1]–[4], which offers a novel design paradigm by adding new degrees of freedom to intelligently control wireless channels for improved communications. Specifically, an RIS is an array composed of massive passive elements, which reflect electromagnetic signals in a desired manner so as to reconfigure the wireless environment [5]. Thanks to its

high array gain, low cost, low power, and low noise [5]–[7], RIS is expected to improve channel capacity [8], extend coverage [9], and reduce power consumption [10] for future 6G communications. Additionally, RISs are projected to have other applications such as in WiFi [11], precision measurement [12], and navigation [13].

Due to the negligible noise introduced by passive RISs, one of the most essential benefits of RISs is the “square-law” array gain. In particular, the array gain of an N -element RIS is proportional to N^2 , which is N times larger than that achievable by the standard massive multiple-input multiple-output (MIMO) [5]. Benefiting from this advantage, RIS is expected to bring significant capacity gains in future 6G wireless networks. However, actually significant capacity gains are only observed in atypical communication scenarios where the direct link from the transmitter to the receiver is completely blocked or very weak [8]–[10], [14]–[16]. By contrast, in the typical scenario where the direct link is not weak, the common RISs with hundreds of passive elements can only achieve negligible capacity gains [17]. The reason behind this phenomenon is the “double fading” effect introduced by RIS, i.e., the signals received via the reflection link suffer from large-scale fading twice. Particularly, the equivalent path loss of the transmitter-RIS-receiver link is the product (instead of the summation) of the path losses of the transmitter-RIS link and RIS-receiver link, which is usually thousands of times larger than that of the direct link [17]. As a result, the “double fading” effect makes it almost impossible for passive RIS to achieve a noticeable capacity gain in typical wireless environment. Most existing works on RIS have bypassed this effect by only considering atypical scenarios with very poor direct links [8]–[10], [14]–[16]. Therefore, to advance the practicability of RIS for future 6G wireless networks, a critical issue must to be addressed is: *How to overcome the fundamental limit of “double fading” effect of RIS?*

To break the fundamental physical limit of the “double fading” effect, the new concept of active RIS is proposed in this paper. Specifically, our contributions are summarized as follows:

- We propose the concept of *active* RIS to overcome the “double fading” effect in typical communication scenarios. Different from the existing *passive* RIS that just passively reflects signals without amplification, the key feature of active RIS is the capability of actively reflecting signals with amplification at the expense of additional power consumption.
- We develop a new signal model for the proposed active RIS, which characterizes how the incident signal is amplified and how non-negligible thermal noise is introduced at the active elements. Particularly, an active RIS element

Z. Zhang, L. Dai, X. Chen, C. Liu, and F. Yang are with the Department of Electronic Engineering as well as the Beijing National Research Center for Information Science and Technology (BNRist), Tsinghua University, Beijing 100084, China (e-mails: zhangzij15@mails.tsinghua.edu.cn, daill@tsinghua.edu.cn, cxb17@mails.tsinghua.edu.cn, liuch17@mails.tsinghua.edu.cn, fan_yang@tsinghua.edu.cn).

R. Schober is with the Institute for Digital Communications at Friedrich-Alexander University Erlangen-Nürnberg (FAU) (e-mail: robert.schober@fau.de).

H. V. Poor is with the Department of Electrical and Computer Engineering, Princeton University, USA (e-mail: poor@princeton.edu).

This work was supported in part by the National Key Research and Development Program of China (Grant No. 2020YFB1807201), in part by the National Natural Science Foundation of China (Grant No. 62031019), and in part by the U.S. National Science Foundation under Grants CCF-0939370 and CCF-1908308.

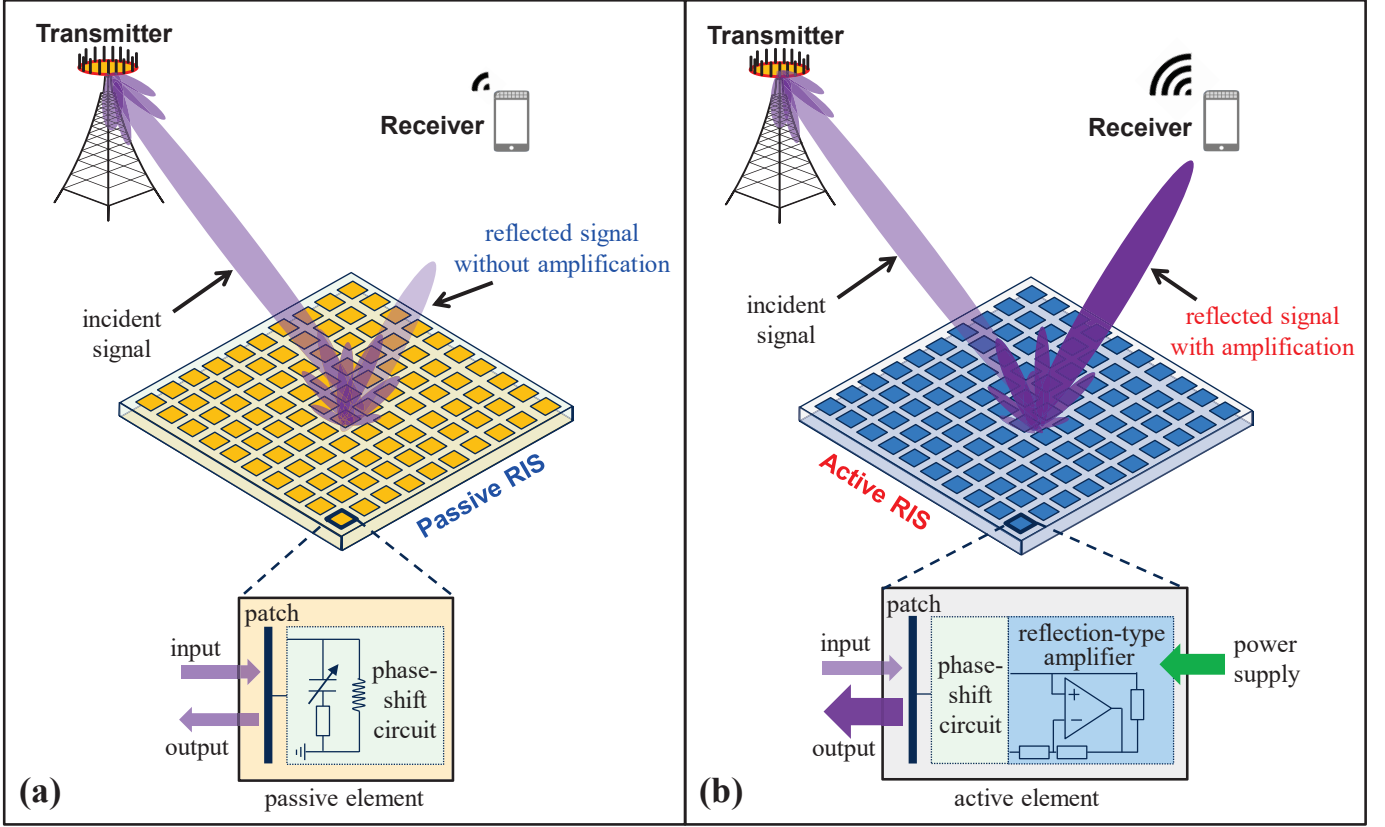


Fig. 1. Comparison between the existing passive RIS (a) and the proposed active RIS (b).

was designed and fabricated to validate the developed signal model through experimental measurements.

- Based on the proposed signal model, we analyze the capacity gain achievable by active RISs and formulate a capacity maximization problem in an active RIS aided MIMO system. Then, a joint transmit and reflect precoding algorithm is proposed to solve this problem. Extensive results show that, in a typical communication scenario, the existing passive RIS only achieves a negligible capacity gain of 3%, while the proposed active RIS is able to achieve a noticeable capacity gain of 129%, thus overcoming the fundamental limit of “double fading” effect.

The rest of this paper is organized as follows. In Section II, the concept of active RIS is introduced and its impact on channel capacity is analyzed. Then, the proposed joint precoding design for capacity maximization is provided in Section III. In Section IV, the results of experimental measurements and numerical simulations are presented. Finally, conclusions are drawn and future works are discussed in Section V.

Notations: \mathbb{C} and \mathbb{R}_+ denote the sets of complex and positive real numbers, respectively; $[\cdot]^{-1}$, $[\cdot]^T$, and $[\cdot]^H$ denote the inverse, transpose, and conjugate-transpose operations, respectively; $\|\cdot\|$ denotes the Euclidean norm of its argument; $\text{diag}(\cdot)$ denotes diagonal operation; $\Re\{\cdot\}$ denotes the real part of its argument; \otimes denotes the Kronecker product; $\angle[\cdot]$ denotes the angle of its complex argument; $\ln(\cdot)$ denotes the natural logarithm of its argument; $\mathcal{CN}(\mu, \Sigma)$ denotes the complex

multivariate Gaussian distribution with mean μ and variance Σ ; \mathbf{I}_L is an $L \times L$ identity matrix, and $\mathbf{0}_L$ is an $L \times 1$ zero vector.

II. CONCEPT OF ACTIVE RIS

We propose the concept of active RIS in this section. First, we briefly review the existing passive RIS, and point out its fatal problem of the “double fading” effect. Then, we propose the concept of active RIS together with its hardware structure and signal model to overcome this fatal problem. Finally, we analyze the capacity gain enabled by active RIS and compare it with that of the existing passive RIS.

A. Existing Passive RIS

The RISs widely studied in existing works are actually passive RISs [1]–[10]. Specifically, as shown in Fig. 1 (a), a passive RIS comprises a large number of passive elements each being able to reflect the incident signal with a controllable phase shift. Each passive RIS element consists of a reflective patch terminated with an impedance-adjustable circuit for phase shifting [1], [4], [18]. Thanks to its passive mode of operation, a passive RIS element practically consumes zero direct-current power [18], and the introduced thermal noise is also negligible [5]–[10]. Thereby, the signal model of an N -element passive RIS widely used in the literature is given as follows [6]

$$\mathbf{y} = \Theta \mathbf{x}, \quad (1)$$

where $\mathbf{x} \in \mathbb{C}^N$ denotes the incident signal, $\mathbf{\Theta} \triangleq \text{diag}(e^{j\theta_1}, \dots, e^{j\theta_N}) \in \mathbb{C}^{N \times N}$ denotes the phase shift matrix of the RIS, and $\mathbf{y} \in \mathbb{C}^N$ denotes the signal reflected by the RIS. Note that no noise is considered in (1). Then, by properly adjusting $\mathbf{\Theta}$ to manipulate the N signals reflected by the N RIS elements to coherently add up with the same phase at the receiver, a high array gain proportional to N^2 can be achieved. This fact is expected to significantly increase the receiver signal-to-noise ratio (SNR) and thus the corresponding system capacity [5]–[7], which is the key reason why RIS has attracted tremendously increasing research interest recently [8]–[16].

Unfortunately, actually this expected high capacity gain can be hardly achieved in typical communication scenarios, where the direct link between the transmitter and the receiver is not such weak. The reason for this result is the “double fading” effect, as the transmitted signal suffers from large-scale fading first in the transmitter-RIS link and then again in the RIS-receiver link. As a result, the equivalent path loss of the transmitter-RIS-receiver reflection link is the product (instead of the summation) of the path losses of the transmitter-RIS link and RIS-receiver link, which is hundreds or even thousands of times larger than that of the unobstructed direct link. Thereby, for RIS to have a noticeable impact on system capacity, thousands or even millions of RIS elements are required to compensate for this extremely large path loss. For example, let’s consider a single-input single-output (SISO) system aided by a passive RIS with the element spacing of a half of a wavelength [19]. Let $d = 200$ m, $d_t = 150$ m, and $d_r = 200$ m denote the distances between transmitter and receiver, transmitter and RIS, RIS and receiver, respectively. For carrier frequencies of 5/10/20 GHz, according to the “double fading” model of RIS [17], $N = 10000/20000/40000$ RIS elements are required to make the reflection link as strong as the direct link. Due to the high overhead of N pilots for channel estimation [20] and the high complexity of $\mathcal{O}(N^2)$ for real-time beamforming [21], such a large number of RIS elements makes the application of passive RIS in practical wireless networks almost impossible [17]. Consequently, most existing works have bypassed the “double fading” effect by only considering the atypical scenario where the direct link is completely blocked or very weak [5]–[10], [14]–[16].

B. Proposed Active RIS

To break the fundamental physical limit of the “double fading” effect, we propose the concept of active RISs as a promising solution to achieve noticeable capacity gains also in typical communication scenarios. As shown in Fig. 1 (b), similar to the existing passive RIS, active RIS can also reflect the incident signals with reconfigurable phase shifts. Different from passive RIS that just reflects signals without amplification, active RIS can further amplify the reflected signals. To achieve this goal, the key component of an active RIS element is the additionally integrated active reflection-type amplifier, which can be realized by many existing active components, such the current-inverting converter [22], the asymmetric current mirror [23], or even some integrated chips [24]. With the reflection-type amplifier supported by a power

supply, the reflected and amplified signal of an N -element active RIS can be modeled as follows¹

$$\mathbf{y} = \underbrace{\mathbf{P}\mathbf{\Theta}\mathbf{x}}_{\text{Desired signals}} + \underbrace{\mathbf{P}\mathbf{\Theta}\mathbf{v}}_{\text{Dynamic noise}} + \underbrace{\mathbf{n}_s}_{\text{Static noise}}, \quad (2)$$

where $\mathbf{P} \triangleq \text{diag}(p_1, \dots, p_N) \in \mathbb{R}_+^{N \times N}$ denotes the amplification factor matrix of the active RIS, wherein each element can be larger than one thanks to the integrated active amplifier. Due to the use of active components, active RISs consume additional power to amplify the reflected signals, and the thermal noise introduced by active RIS elements cannot be ignored as is done for passive RIS. Particularly, as shown in (2), the introduced noises can be divided into dynamic noise and static noise [23]. Specifically, \mathbf{v} is related to the input noise and noise factor of the active RIS elements [23], while the static noise \mathbf{n}_s is unrelated to \mathbf{P} and is usually negligible compared with the dynamic noise $\mathbf{P}\mathbf{\Theta}\mathbf{v}$ [23]. Without loss of generality, here we assume $\mathbf{v} \sim \mathcal{CN}(\mathbf{0}_N, \sigma_v^2 \mathbf{I}_N)$.

Then, we consider an active RIS aided multiple-input multiple-output (MIMO) system, where an M -antenna base station (BS) simultaneously serve K single-antenna users with the aid of an N -element active RIS. Therefore, according to (2), the signal $r_k \in \mathbb{C}$ received at user k can be modeled as

$$r_k = \underbrace{(\mathbf{h}_k^H)}_{\text{Direct link}} + \underbrace{(\mathbf{f}_k^H \mathbf{P} \mathbf{\Theta} \mathbf{G})}_{\text{Reflection link}} \sum_{j=1}^K \mathbf{w}_j s_j + \underbrace{\mathbf{f}_k^H \mathbf{P} \mathbf{\Theta} \mathbf{v}}_{\text{Noises introduced at active RIS}} + \underbrace{z_k}_{\text{Noise introduced at user } k}, \quad (3)$$

where $\mathbf{s} \triangleq [s_1, \dots, s_K]^T \in \mathbb{C}^K$ denote the transmitted symbols for K users with normalized power; $\mathbf{G} \in \mathbb{C}^{N \times M}$, $\mathbf{h}_k^H \in \mathbb{C}^{1 \times M}$, and $\mathbf{f}_k^H \in \mathbb{C}^{1 \times N}$ denote the channels from BS to RIS, from BS to user k , and from RIS to user k , respectively; $\mathbf{w}_k \in \mathbb{C}^{M \times 1}$ denotes the BS beamforming vector for s_k ; z_k denotes the additive white Gaussian noise (AWGN) at the user and here we assume $z_k \sim \mathcal{CN}(0, \sigma^2)$.

It should be noted that, the proposed active RIS is fundamentally different from the RIS equipped with active radio-frequency (RF) components [25], [26]. Specifically, some passive RIS elements are connected to additional active RF chains, which are used for baseband signal processing. In this way, these RIS elements are enabled to have the signal processing capabilities [25], [26]. On the contrary, the proposed active RIS has no these capabilities, which only reflects and amplifies the incident signal to strengthen the reflection link. Besides, although the proposed active RIS can amplify the incident signal, which is similar to the full-duplex amplify-and-forward (FD-AF) relay, their hardware structures and transmission models are actually quite different. Specifically, FD-AF relay is equipped with RF chains to receive the incident signal and then transmit it after amplification [27]. Due to the long delay of this process, it takes two time slots to complete the transmission of a symbol, and the received signal at the receiver in a time slot actually carries two different symbols, which are transmitted by the transmitter and the FD-AF relay,

¹This signal model will be verified by experimental measurements in Subsection IV-A.

respectively [27]. Thus, FD-AF has two different transmission models in two adjacent time slots [27, Eq. (22), Eq. (25)], while the proposed active RIS has only one transmission model (3) in every time slot.

To illustrate how active RIS can overcome the “double fading” effect, the capacity gain achievable by active RIS will be analyzed based on the new signal model (2) in the next subsection.

C. Performance Analysis

We consider to analyze the capacity gain achievable by active RIS by studying the user’s achievable SNR in a simple SISO scenario. To focus on the capacity gain provided by the active RIS aided reflection link, we ignore the direct link by setting $\mathbf{h}_k \triangleq \mathbf{0}$ [28]. For simplicity, we assume that every active RIS element has the same amplification factor ($p_n \triangleq p$, $\forall n \in \{1, \dots, N\}$), and redefine $\mathbf{G} \triangleq \mathbf{g} = [g_1, \dots, g_N]^T$, $\mathbf{f}_k \triangleq \mathbf{f} = [f_1, \dots, f_N]^T$, and $\mathbf{w}_k \triangleq w$. Then, according to (3), the maximization of the user’s SNR γ subject to the power constraints at the BS and active RIS can be formulated as follows

$$\begin{aligned} \max_{w, p, \Theta} \quad & \gamma = \frac{|p\mathbf{f}^H \Theta \mathbf{g} w|^2}{p^2 \|\mathbf{f}^H \Theta\|^2 \sigma_v^2 + \sigma^2} \\ \text{s.t.} \quad & C_1 : |w|^2 \leq P_{\text{BS}}^{\max} \\ & C_2 : p^2 \|\Theta \mathbf{g} w\|^2 + p^2 \|\Theta\|^2 \sigma_v^2 \leq P_A^{\max}, \end{aligned} \quad (4)$$

where P_{BS}^{\max} and P_A^{\max} denote the maximum transmit power and reflect power at the BS and active RIS, respectively.

The optimal solution to problem (4) can be obtained by the Lagrange multiplier method as follows

$$w^{\text{opt}} = \sqrt{P_{\text{BS}}^{\max}}, \quad (5a)$$

$$\theta_n^{\text{opt}} = \angle f_n + \angle g_n, \quad \forall n \in \{1, \dots, N\}, \quad (5b)$$

$$p^{\text{opt}} = \sqrt{\frac{P_A^{\max}}{\sum_{n=1}^N |g_n|^2 + \sigma_v^2}}. \quad (5c)$$

By substituting (5) into (4), the user’s maximum SNR for active RIS is obtained as

$$\gamma_{\text{active}} = \frac{P_{\text{BS}}^{\max} P_A^{\max} \left| \sum_{n=1}^N |f_n| |g_n| \right|^2}{P_A^{\max} \sigma_v^2 \sum_{n=1}^N |f_n|^2 + \sigma^2 \left(\sum_{n=1}^N |g_n|^2 + \sigma_v^2 \right)}. \quad (6)$$

Then, assume $\mathbf{f} \sim \mathcal{CN}(\mathbf{0}_N, \varrho_f^2 \mathbf{I}_N)$ and $\mathbf{g} \sim \mathcal{CN}(\mathbf{0}_N, \varrho_g^2 \mathbf{I}_N)$. By letting $N \rightarrow \infty$ for (6), according to law of large numbers, we can further derive the asymptotic SNR of active RIS from (6) as

$$\gamma_{\text{active}} \rightarrow N \frac{P_{\text{BS}}^{\max} P_A^{\max} \pi^2 \varrho_f^2 \varrho_g^2}{16 \left(P_A^{\max} \sigma_v^2 \varrho_f^2 + \sigma^2 \varrho_g^2 \right)}. \quad (7)$$

We can observe from (7) that, compared with the asymptotic SNR of passive RIS given as [5]

$$\gamma_{\text{passive}} \rightarrow N^2 \frac{P_{\text{BS}}^{\max} \pi^2 \varrho_f^2 \varrho_g^2}{16 \sigma^2}, \quad (8)$$

which is proportional to N^2 , the asymptotic SNR of the active RIS γ_{active} is proportional to N due to the noises additionally

introduced by the use of active components. At first glance, it seems that the SNR proportional to N^2 of passive RIS exceeds the SNR of active RIS, which is proportional to N . However, actually the opposite is true, as will be explained in detail in the following.

The reason behind this counterintuitive behavior is that, because of the use of reflection-type amplifier in active RIS, only when N is unaffordably large can passive RISs outperform active RISs, which is unrealistic in practical systems. Specifically, assuming N is large, by solving $\gamma_{\text{passive}} \geq \gamma_{\text{active}}$ according to (7) and (8), the required number N for the passive RIS to outperform the active RIS has to satisfy

$$N \geq \frac{P_A^{\max} \sigma^2}{P_A^{\max} \sigma_v^2 \varrho_f^2 + \sigma^2 \varrho_g^2}. \quad (9)$$

For example, when $P_{\text{BS}}^{\max} = P_A^{\max} = 0$ dBW, $\sigma^2 = \sigma_v^2 = -90$ dBm [9], and the path loss of \mathbf{g} and \mathbf{f} are both -80 dB with Rayleigh fading, the required N is 5×10^7 according to (9), which is almost impossible to realize in practice. Conversely, for a more practical number of $N = 256$, according to (7) and (8), the SNR achieved by passive RIS is $\gamma_{\text{passive}} \approx 6.1$ dB, while the SNR achieved by active RIS is $\gamma_{\text{active}} \approx 59.0$ dB, which is about 2.3×10^5 times higher than γ_{passive} .

It should be pointed out that, although additional thermal noises are introduced by the active components, active RIS can still achieve the improved SNR. The reason is that, the desired signals of multiple active RIS elements can be coherently added up with the same phase at the user, while the introduced noises cannot.

III. JOINT TRANSMIT AND REFLECT PRECODING DESIGN

To investigate the capacity gain of the proposed active RIS in typical communication scenarios, in this section, we further extend the SISO case studied in Section II to the more general MIMO case. Specifically, we first formulate the problem to maximize the system capacity in an active RIS aided MIMO system. Then, we propose a joint precoding algorithm to solve the problem.

A. Problem Formulation

Firstly, we formulate the optimization problem for maximizing the capacity in an active RIS aided MIMO system. According to the signal model for the MIMO system in (2), the signal-to-interference-plus-noise ratio (SINR) at the user k can be derived as

$$\gamma_k = \frac{|\mathbf{H}_k^H \mathbf{w}_k|^2}{\sum_{j=1, j \neq k}^K |\mathbf{H}_k^H \mathbf{w}_j|^2 + \|\mathbf{f}_k^H \mathbf{P} \Theta\|^2 \sigma_v^2 + \sigma^2}, \quad (10)$$

wherein $\mathbf{H}_k^H = \mathbf{h}_k^H + \mathbf{f}_k^H \mathbf{P} \Theta \mathbf{G} \in \mathbb{C}^{1 \times M}$ is the equivalent channel from the BS to user k . Therefore, subject to the power constraints at the BS and the active RIS, the capacity maximization problem can be formulated as follows

$$\begin{aligned} \max_{\mathbf{w}, \mathbf{P}, \Theta} \quad & R_{\text{sum}} = \sum_{k=1}^K \log_2(1 + \gamma_k) \\ \text{s.t.} \quad & C_1 : \sum_{k=1}^K \|\mathbf{w}_k\|^2 \leq P_{\text{BS}}^{\max} \end{aligned} \quad (11)$$

Algorithm 1 Proposed Joint Precoding Algorithm

Input: The channels \mathbf{G} , \mathbf{h}_k , and \mathbf{f}_k , $\forall k \in \{1, \dots, K\}$.
Output: Optimized \mathbf{W} , \mathbf{P} , $\mathbf{\Theta}$, and sum-rate R_{sum} .
 1: Initialize \mathbf{W} , \mathbf{P} and $\mathbf{\Theta}$;
 2: **while** no convergence of R_{sum} **do**
 3: Update ρ by (13);
 4: Update ϖ by (14);
 5: Update \mathbf{W} by solving (15);
 6: Update $\mathbf{\Psi}$ by solving (16);
 7: **end while**
 8: Obtain \mathbf{P} and $\mathbf{\Theta}$ from $\mathbf{\Psi}$;
 9: **return** Optimized \mathbf{W} , \mathbf{P} , $\mathbf{\Theta}$, and R_{sum} .

$$C_2 : \sum_{k=1}^K \|\mathbf{P}\mathbf{\Theta}\mathbf{G}\mathbf{w}_k\|^2 + \|\mathbf{P}\mathbf{\Theta}\|^2 \sigma_v^2 \leq P_A^{\max},$$

where $\mathbf{W} \triangleq [\mathbf{w}_1^T, \dots, \mathbf{w}_K^T]^T$. Due to the non-convex objective function of the problem (11), the joint design of \mathbf{W} , \mathbf{P} , and $\mathbf{\Theta}$ is challenging. To efficiently solve the problem, a joint precoding algorithm design based on alternating optimization will be proposed in the next subsection.

B. Proposed Joint Precoding Algorithm

In (11), \mathbf{P} and $\mathbf{\Theta}$ always appear in product form, thus \mathbf{P} and $\mathbf{\Theta}$ can be merged as $\mathbf{\Psi} = \mathbf{P}\mathbf{\Theta} = \text{diag}(p_1 e^{j\theta_1}, \dots, p_N e^{j\theta_N}) \in \mathbb{C}^{N \times N}$. Then, to deal with the sum-of-logarithm and fractions in (11), we exploit fractional programming [29] to decouple the optimization problem (11). Specifically, by introducing auxiliary variables $\rho \triangleq [\rho_1, \dots, \rho_K]$ and $\varpi \triangleq [\varpi_1, \dots, \varpi_K] \in \mathbb{C}^K$, the original problem (11) can be equivalently reformulated as follows

$$\begin{aligned} \max_{\mathbf{W}, \mathbf{\Psi}, \rho, \varpi} \quad & R'_{\text{sum}}(\mathbf{W}, \mathbf{\Psi}, \rho, \varpi) = \sum_{k=1}^K \ln(1 + \rho_k) - \\ & \sum_{k=1}^K \rho_k + \sum_{k=1}^K g_k(\mathbf{W}, \mathbf{\Psi}, \rho_k, \varpi_k) \quad (12) \\ \text{s.t.} \quad & C_1 : \|\mathbf{W}\|^2 \leq P_{\text{BS}}^{\max} \\ & C_2 : \sum_{k=1}^K \|\mathbf{\Psi}\mathbf{G}\mathbf{w}_k\|^2 + \|\mathbf{\Psi}\|^2 \sigma_v^2 \leq P_A^{\max}, \end{aligned}$$

where

$$g_k(\mathbf{W}, \mathbf{\Psi}, \rho_k, \varpi_k) = 2\sqrt{(1 + \rho_k)} \Re\{\varpi_k^* \mathbf{H}_k^H \mathbf{w}_k\} - |\varpi_k|^2 \left\{ \sum_{j=1}^K |\mathbf{H}_k^H \mathbf{w}_j|^2 + \|\mathbf{f}_k^H \mathbf{\Psi}\|^2 \sigma_v^2 + \sigma^2 \right\}.$$

Then, according to the strong convergence of FP methods proved in [29], the solution to (12) can be achieved by alternately optimizing \mathbf{W} , $\mathbf{\Psi}$, ρ , and ϖ in (12), until R_{sum} converges. For clarity, we summarize the proposed joint precoding algorithm in **Algorithm 1**, and the optimal solutions to these variables are given in the following four steps, respectively.

1) *Fix $(\mathbf{W}, \mathbf{\Psi}, \varpi)$ and optimize ρ* : By solving $\frac{\partial R'_{\text{sum}}}{\partial \rho_k} = 0$ for (12), the optimal ρ can be obtained as

$$\rho_k^{\text{opt}} = \frac{\xi^2 + \xi \sqrt{\xi^2 + 4}}{2}, \quad \forall k \in \{1, \dots, K\}, \quad (13)$$

where $\xi = \Re\{\varpi_k^* \mathbf{H}_k^H \mathbf{w}_k\}$.

2) *Fix $(\mathbf{W}, \mathbf{\Psi}, \rho)$ and optimize ϖ* : By solving $\frac{\partial R'_{\text{sum}}}{\partial \varpi_k} = 0$ for (12), the optimal ϖ is given by

$$\varpi_k^{\text{opt}} = \frac{\sqrt{(1 + \rho_k)} \mathbf{H}_k^H \mathbf{w}_k}{\sum_{j=1}^K |\mathbf{H}_k^H \mathbf{w}_j|^2 + \|\mathbf{f}_k^H \mathbf{\Psi}\|^2 \sigma_v^2 + \sigma^2}, \quad \forall k \in \{1, \dots, K\}. \quad (14)$$

3) *Fix $(\mathbf{\Psi}, \rho, \varpi)$ and optimize \mathbf{W}* : By defining

$$\begin{aligned} \mathbf{b}_k^H &= 2\sqrt{(1 + \rho_k)} \varpi_k^* \mathbf{H}_k^H, \quad \mathbf{b} = [\mathbf{b}_1^T, \mathbf{b}_2^T, \dots, \mathbf{b}_N^T]^T, \\ \mathbf{A} &= \mathbf{I}_K \otimes \sum_{k=1}^K |\varpi_k|^2 \mathbf{H}_k \mathbf{H}_k^H, \quad \mathbf{\Xi} = \mathbf{I}_K \otimes \{\mathbf{G}^H \mathbf{\Psi}^H \mathbf{\Psi} \mathbf{G}\}, \\ P_m^{\max} &= P_A^{\max} - \|\mathbf{\Psi}\|^2 \sigma_v^2, \end{aligned}$$

the problem (12) can be reformulated as follows

$$\begin{aligned} \max_{\mathbf{W}} \quad & \Re\{\mathbf{b}^H \mathbf{W}\} - \mathbf{W}^H \mathbf{A} \mathbf{W} \\ \text{s.t.} \quad & C_1 : \|\mathbf{W}\|^2 \leq P_{\text{BS}}^{\max} \\ & C_2 : \mathbf{W}^H \mathbf{\Xi} \mathbf{W} \leq P_m^{\max}, \end{aligned} \quad (15)$$

which is a standard quadratic constraint quadratic programming (QCQP) problem. Thus, the optimal \mathbf{w}^{opt} can be directly obtained with existing optimization methods such as the alternating direction method of multipliers (ADMM) [30].

4) *Fix $(\mathbf{W}, \rho, \varpi)$ and optimize $\mathbf{\Psi}$* : By defining $\psi = [p_1 e^{j\theta_1}, \dots, p_N e^{j\theta_N}]^H$, problem (12) can be reformulated as follows

$$\begin{aligned} \max_{\mathbf{\Psi}} \quad & \Re\{\psi^H \mathbf{v}\} - \psi^H \mathbf{\Omega} \psi \\ \text{s.t.} \quad & C_2 : \psi^H \mathbf{\Pi} \psi \leq P_A^{\max}, \end{aligned} \quad (16)$$

wherein

$$\begin{aligned} \mathbf{v} &= 2 \sum_{k=1}^K \sqrt{(1 + \rho_k)} \text{diag}(\varpi_k^* \mathbf{f}_k^H) \mathbf{G} \mathbf{w}_k - \sum_{k=1}^K |\varpi_k|^2 \text{diag}(\mathbf{f}_k^H) \mathbf{G} \sum_{j=1}^K \mathbf{w}_j \mathbf{w}_j^H \mathbf{h}_k, \\ \mathbf{\Omega} &= \sum_{k=1}^K |\varpi_k|^2 \text{diag}(\mathbf{f}_k^H) \text{diag}(\mathbf{f}_k) \sigma_v^2 + \sum_{k=1}^K |\varpi_k|^2 \sum_{j=1}^K \text{diag}(\mathbf{f}_k^H) \mathbf{G} \mathbf{w}_j \mathbf{w}_j^H \mathbf{G}^H \text{diag}(\mathbf{f}_k), \\ \mathbf{\Pi} &= \sum_{k=1}^K \text{diag}(\mathbf{G} \mathbf{w}_k) (\text{diag}(\mathbf{G} \mathbf{w}_k))^H + \sigma_v^2 \mathbf{I}_N. \end{aligned}$$

Note that (16) is also a standard QCQP problem, which can be alternately solved by existing optimization methods such as ADMM [30].

IV. VALIDATION RESULTS

In this section, we present the results for the developed signal model, the performance analyses, and the joint precoding design for the proposed active RIS.

A. Validation Results for Signal Model

To validate the developed signal model (2), we designed and fabricated an active RIS element with integrated reflection-type amplifier for experimental measurements² in [31]. Note

²In October 2019, we start to design an active RIS element integrating a reflection-type amplifier. Then, the fabrication of this active RIS element was finished in August 2020. Subsequently, we set out to establish an experimental environment for the signal measurements on this element, and all measurements were completed in February 2021.

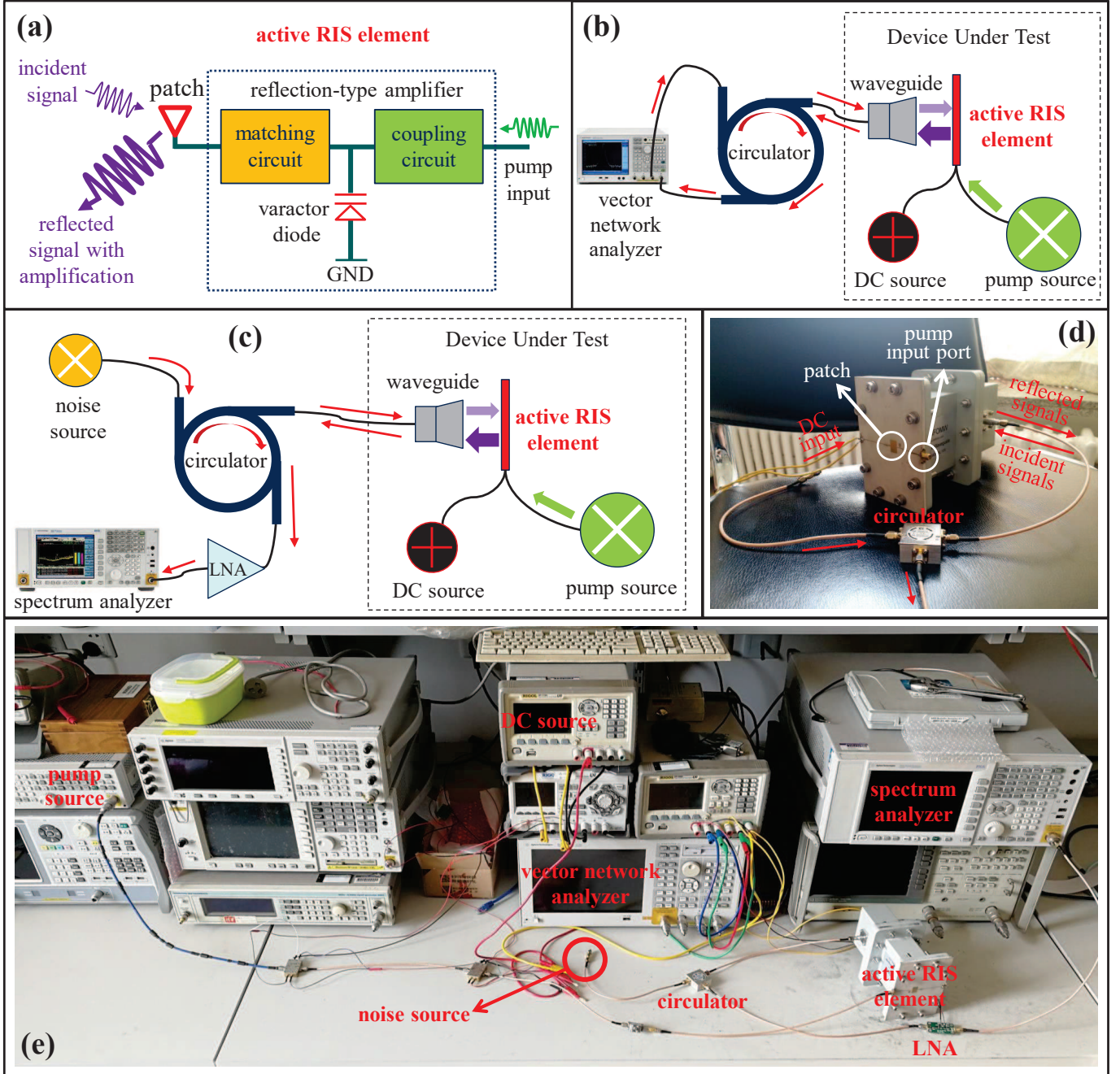


Fig. 2. The experimental devices and environment for validating the developed signal model (2) of the proposed active RIS.

that this design can be directly extended to the large-array case [18]. Particularly, since the phase-shifting ability of RIS has been widely verified [18], we focus on studying the reflection gain and the noise introduced by active RIS. Thereby, the validation of (2) is equivalent to validating

$$P_y = \underbrace{GP_x}_{\text{Desired-signal power}} + \underbrace{G\sigma_v^2 + \sigma_s^2}_{\text{noise power}}, \quad (17)$$

where P_x is the power of the incident signal; $p^2 \equiv G$ is the reflection gain of the active RIS element; $G\sigma_v^2$ and σ_s^2 are the dynamic and static noise powers at the RIS element, respectively; P_y is the power of the reflected signals.

To validate the signal model (17), we first establish the systems for experimental measurements as illustrated in Fig. 2.

Specifically, Fig. 2 (a) illustrates the structure of the fabricated active RIS element operating at a frequency of 2.36 GHz [31]. The incident signal and the pump input are coupled in a varactor-diode-based reflection-type amplifier to generate the reflected signal with amplification. Fig. 2 (b) illustrates the system used for measuring the reflection gain of the active RIS element. A direct-current (DC) source is used to provide a bias voltage of 7.25V for driving the active RIS element, and a pump source is used to control the reflection gain. A circulator is used to separate the incident signal and the reflected signal, and the reflection gain is directly measured by a vector network analyzer. Fig. 2 (c) illustrates the system for measuring the noises introduced at the active RIS element, where a spectrum analyzer is used to measure the noise power.

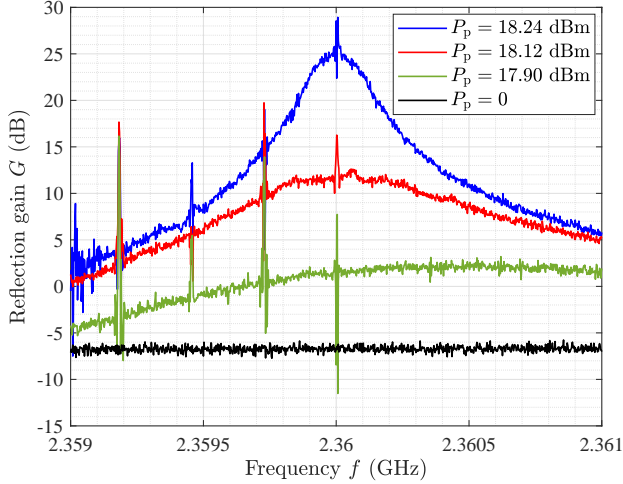
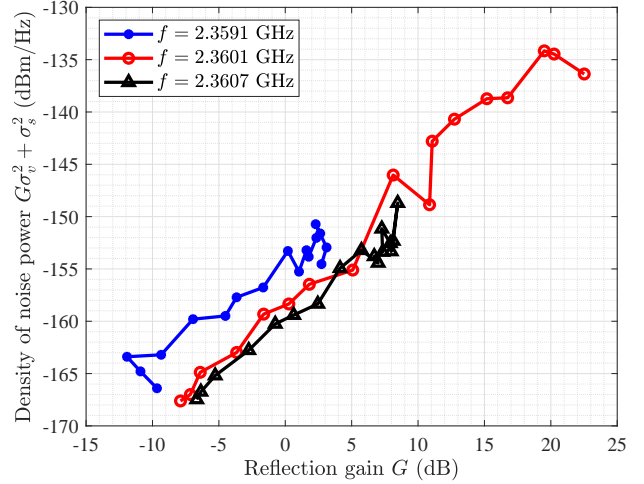
(a) The reflection gain G vs. the signal frequency f .(b) The noise power $G\sigma_v^2 + \sigma_s^2$ vs. the reflection gain G .

Fig. 3. The experimental measurement results for the signal model of active RIS.

The noise source is a 50Ω impedance for simulating an input noise of -174 dBm/Hz at each patch. The reflected signal is amplified by a low-noise amplifier (LNA) so that the spectrum analyzer can detect it. Fig. 2 (d) shows a photo of the fabricated active RIS element under test, which is connected by a waveguide for signal exchanges. Fig. 2 (e) is a photo of the experimental environment with the required equipment for device driving and signal measurement. Based on the established measurement systems, the measurement results are presented as follows.

Using the measurement system for reflection gain depicted in Fig. 2 (b), we first investigate the reflection gain G of the active RIS element. Note that the reflection gain G is controlled by the input power of the pump source P_p . By setting the input power of the vector network analyzer as $P_x = -50$ dBm, the reflection gain G as a function of the signal frequency can be directly measured via the vector network analyzer. Then, in Fig. 3 (a), we show the measurement results of the reflection gain G as a function of the signal frequency f with different powers of the pump inputs P_p . We can observe that the active RIS element can achieve a reflection gain G higher than 25 dB when $P_p = 18.24$ dBm, which verifies the efficient reflection gain of active RIS. On the other hand, when $P_p = 0$, G falls to -6 dB, which is lower than the expected 0 dB. This result is caused by the inherent power losses of the circulator and transmission lines used for measurements.

Based on the reflection gain G measured above, we further study the noise power introduced by the active RIS element, i.e., $G\sigma_v^2 + \sigma_s^2$ in (17). Using the noise measurement system in Fig. 2 (c), in Fig. 3 (b), we show the measurement results of the power spectrum density of the noise power $G\sigma_v^2 + \sigma_s^2$ as a function of G at different operating frequencies. We can observe that the noise power increases nearly linearly with G , which verifies the noise model $G\sigma_v^2 + \sigma_s^2$ in (17). Particularly, for $f = 2.3601$ GHz, the power spectrum density of σ_s^2 is about -174 dBm/Hz, while that of σ_v^2 is about -160 dBm/Hz, which is about 15 dB higher than σ_s^2 . The reason is that the input noise is amplified by the noise factor [23], and additional

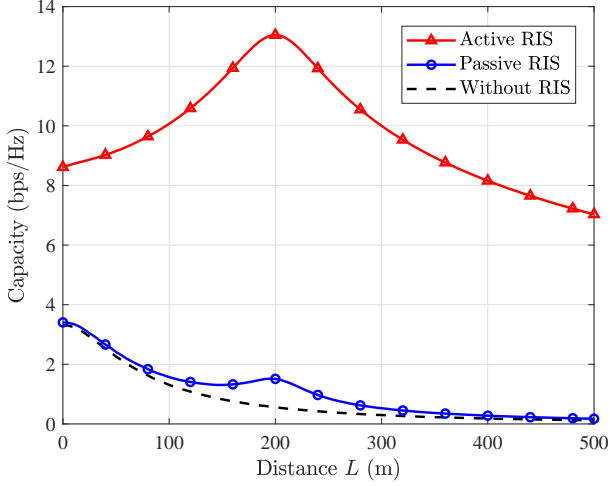
noises are also introduced by other active devices, such as the leakage noise from the DC source.

B. Simulation Results for Performance Analyses

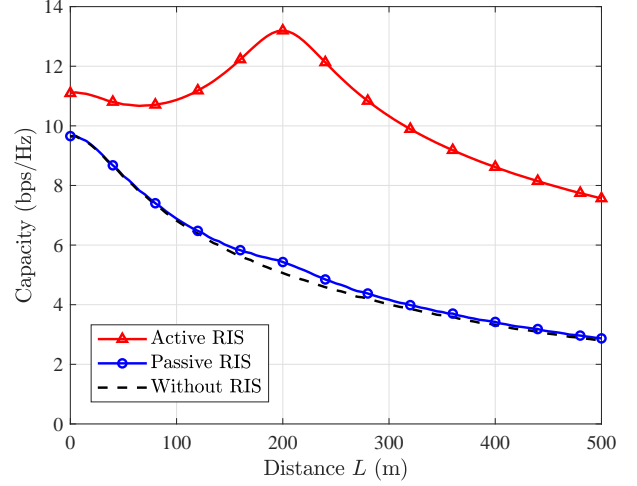
To support the capacity analysis in Section II, in this subsection, we evaluate the capacity of an active RIS aided SISO system through simulations.

For the simulation setup, we consider a 2-D scenario, where a SISO communication system operating at 5 GHz is aided by a 256-element active/passive RIS with an element spacing of a half of a wavelength. The BS, the active/passive RIS, and the user are located at $(0, -40)$ m, $(200, 30)$ m, and $(L, 0)$, respectively. The active RIS employs the optimal precoding design in (5), while passive RIS employs an existing precoding method in [9]. The maximum transmit power at BS and the maximum reflect power at active RIS are set as $P_{BS}^{\max} = P_A^{\max} = 10$ mW. The noise powers at the active RIS and the user are set as $\sigma^2 = \sigma_v^2 = -90$ dBm, and the free-space path loss model [17] with Rayleigh small-scale fading is used to generate all channels. To characterize the case that the direct link is partially blocked, we assume that the channel gain of the partially blocked link is 1% of that of the unobstructed line-of-sight (LoS) [9].

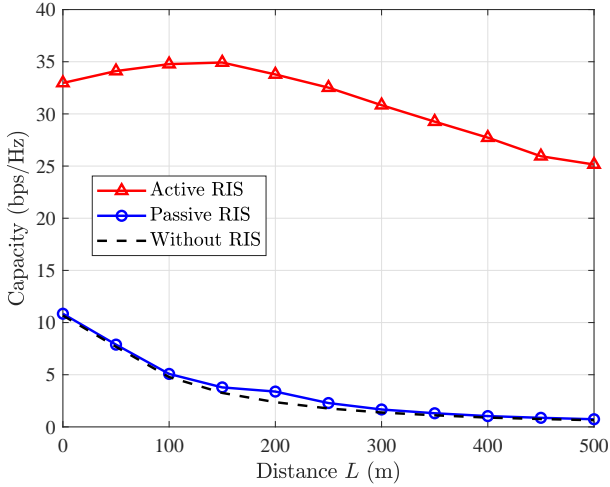
Then, in Fig. 4, we plot the capacity as a function of the distance L in (a) an atypical communication scenario where the direct link is partially blocked and (b) a typical communication scenario with a line-of-sight (LoS) direct link. From this figure, we notice the following two observations. Firstly, in the atypical scenario, where the direct link is partially blocked, the passive RIS can indeed achieve a performance improvement, while the active RIS achieves much higher capacity gain at the cost of additional power consumption. For example, when $L = 200$ m, the capacities without RIS, with passive RIS, and with active RIS are 0.56 bps/Hz, 1.51 bps/Hz, and 13.05 bps/Hz, respectively. At this typical position, compared with the baseline without RIS, the passive RIS achieves a capacity gain of about 170%, while the active RIS achieves a much higher gain of about 2230%. Secondly, in the typical scenario,



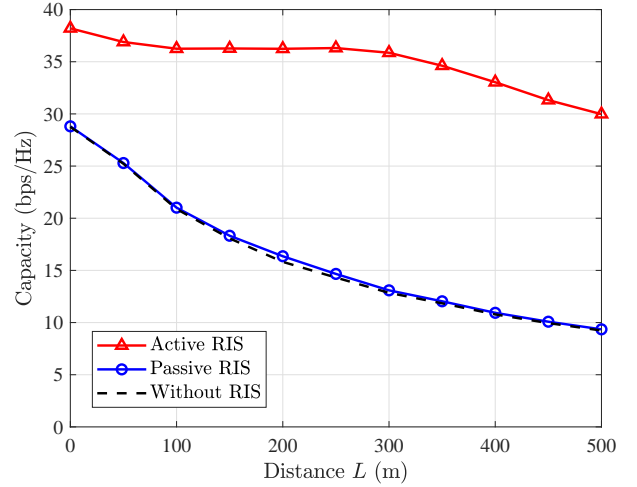
(a) Capacity in an atypical communication scenario.



(b) Capacity in a typical communication scenario.

Fig. 4. Simulation results of the capacity vs. the distance L in an RIS-aided SISO system.

(a) Capacity in the atypical communication scenario.



(b) Capacity in the typical communication scenario.

Fig. 5. Simulation results of the capacity vs. the distance L in an RIS-aided MIMO system.

where the LoS direct link exists, the passive RIS achieves only a negligible capacity gain, while active RIS can still realize a noticeable capacity gain. For example, when $L = 200$ m, the capacity without RIS, with passive RIS, and with active RIS are 5.10 bps/Hz, 5.41 bps/Hz, and 13.19 bps/Hz, respectively. Then, compared with the baseline without RIS, we can calculate that the capacity gain of passive RIS is a negligible 6%, which is caused by the “double fading” effect as we have discussed before. Fortunately, at the cost of additional power consumption, the proposed active RIS can still achieve a noticeable capacity gain of about 159%. Therefore, active RIS can be a promising solution to efficiently overcome the “double fading” effect.

C. Simulation Results for Joint Precoding Design

To evaluate the capacity gain of the proposed active RIS in the more general MIMO communication system and the associated joint precoding algorithm proposed in Section III, in

this subsection, we extend the studied SISO system to a MIMO system and present the corresponding simulation results.

For the simulation setup, we consider a MIMO system operating at 5 GHz, which is composed of an 4-antenna BS, four single-antenna users, and a 1024-element active/passive RIS. The four user are randomly located in a circle with a radius of 5 m from the center $(L, 0)$, and the other system parameters including transmit power and noise power are the same as those used in Subsection IV-B. For the active RIS, the proposed **Algorithm 1** is employed, while for the passive RIS, an existing algorithm in [21] is used.

Then, in Fig. 5, we plot the capacity vs. distance L for both typical and atypical communication scenarios. We can observe that the trends of the results are similar to those in Fig. 4. For example, when $L = 200$ m, the capacities without RIS, with passive RIS, and with active RIS in atypical scenario are 2.37 bps/Hz, 3.90 bps/Hz, and 33.78 bps/Hz respectively, while those in typical scenario are 15.82 bps/Hz, 16.36 bps/Hz, and 36.24 bps/Hz, respectively. At this typical position, passive

RIS provides a 65% gain in the atypical scenario and a negligible 3% gain in the typical scenario. By contrast, active RIS can achieve noticeable capacity gains of 1325% in the atypical scenario and 129% in the typical scenario, which are much higher than those achieved by passive RIS in the corresponding scenarios. These results demonstrate that, compared with the existing passive RIS, the proposed active RIS can overcome the “double fading” effect and achieve noticeable capacity gains in typical communication scenarios.

V. CONCLUSIONS

In this paper, we have proposed the concept of active RIS to break the fundamental limit of the “double fading” effect. Then, we have developed a signal model for active RIS, which has been validated by a fabricated active RIS element through experimental measurements. Based on the proposed signal model, we have analyzed the capacity gain achievable by active RIS and then formulated an optimization problem to maximize the channel capacity in an active RIS aided MIMO system. After that, we have proposed a joint precoding algorithm to solve this problem. Finally, extensive results have showed that, compared with the benchmark without RIS, the existing passive RIS can only realize a negligible capacity gain about 3% in the typical application scenario, while the proposed active RIS can achieve a noticeable capacity gain about 129%, thus overcoming the fundamental limit of “double fading” effect. In the future, more works are calling for further investigation for active RIS, including hardware design [22], prototype development [7], channel estimation [20], energy efficiency analysis [10], etc.

REFERENCES

- [1] L. Zhang, X. Q. Chen, S. Liu, Q. Zhang, J. Zhao, J. Y. Dai, G. D. Bai, X. Wan, Q. Cheng, G. Castaldi, V. Galdi, and T. J. Cui, “Space-time-coding digital metasurfaces,” *Nat. Commun.*, vol. 9, no. 4338, Oct. 2018.
- [2] X. Ni, A. V. Kildishev, and V. M. Shalae, “Metasurface holograms for visible light,” *Nat. Commun.*, vol. 4, no. 2807, Nov. 2013.
- [3] H. Ren, “A light-programmable metasurface,” *Nat. Elect.*, vol. 3, pp. 137–138, Mar. 2020.
- [4] S. Venkatesh, X. Lu, H. Saeidi, and K. Sengupta, “A high-speed programmable and scalable terahertz holographic metasurface based on tiled CMOS chips,” *Nat. Elect.*, vol. 3, pp. 785–793, Dec. 2020.
- [5] M. Di Renzo, A. Zappone, M. Debbah, M. S. Alouini, C. Yuen, J. de Rosny, and S. Tretakov, “Smart radio environments empowered by reconfigurable intelligent surfaces: How it works, state of research, and the road ahead,” *IEEE J. Sel. Areas Commun.*, vol. 38, no. 11, pp. 2450–2525, Nov. 2020.
- [6] E. Basar, M. Di Renzo, J. De Rosny, M. Debbah, M. Alouini, and R. Zhang, “Wireless communications through reconfigurable intelligent surfaces,” *IEEE Access*, vol. 7, pp. 116 753–116 773, Aug. 2019.
- [7] L. Dai, B. Wang, M. Wang, X. Yang, J. Tan, S. Bi, S. Xu, F. Yang, Z. Chen, M. Di Renzo, C. B. Chae, and L. Hanzo, “Reconfigurable intelligent surface-based wireless communications: Antenna design, prototyping, and experimental results,” *IEEE Access*, vol. 8, pp. 45 913–45 923, Mar. 2020.
- [8] C. Huang, R. Mo, and C. Yuen, “Reconfigurable intelligent surface assisted multiuser MISO systems exploiting deep reinforcement learning,” *IEEE J. Sel. Areas Commun.*, vol. 38, no. 8, pp. 1839–1850, Aug. 2020.
- [9] P. Wang, J. Fang, X. Yuan, Z. Chen, and H. Li, “Intelligent reflecting surface-assisted millimeter wave communications: Joint active and passive precoding design,” *IEEE Trans. Veh. Technol.*, vol. 69, no. 12, pp. 14 960–14 973, Dec. 2020.
- [10] C. Huang, A. Zappone, G. C. Alexandropoulos, M. Debbah, and C. Yuen, “Reconfigurable intelligent surfaces for energy efficiency in wireless communication,” *IEEE Trans. Wireless Commun.*, vol. 18, no. 8, pp. 4157–4170, Aug. 2019.
- [11] H. Zhao, Y. Shuang, M. Wei, T. J. Cui, P. Hougne, and L. Li, “Metasurface-assisted massive backscatter wireless communication with commodity Wi-Fi signals,” *Nat. Commun.*, vol. 11, no. 3926, Aug. 2020.
- [12] M. Faraji-Dana, E. Arbabi, A. Arbabi, S. M. Kamali, H. Kwon, and A. Faraon, “Compact folded metasurface spectrometer,” *Nat. Commun.*, vol. 9, no. 4196, Oct. 2013.
- [13] J. Park, B. G. Jeong, S. I. Kim, D. Lee, J. Kim, C. Shin, C. B. Lee, T. Otsuka, J. Kyoung, S. Kim, K. Yang, Y. Park, J. Lee, I. Hwang, J. Jang, S. H. Song, M. L. Brongersma, K. Ha, S. Hwang, H. Choo, and B. L. Choi, “All-solid-state spatial light modulator with independent phase and amplitude control for three-dimensional LiDAR applications,” *Nat. Nanotechnol.*, vol. 16, p. 69–76, Oct. 2020.
- [14] W. Zhao, G. Wang, S. Atapattu, T. A. Tsiftsis, and C. Tellambura, “Is backscatter link stronger than direct link in reconfigurable intelligent surface-assisted system?” *IEEE Commun. Lett.*, vol. 24, no. 6, pp. 1342–1346, Jun. 2020.
- [15] T. Hou, Y. Liu, Z. Song, X. Sun, and Y. Chen, “MIMO-NOMA networks relying on reconfigurable intelligent surface: A signal cancellation-based design,” *IEEE Trans. Commun.*, vol. 68, no. 11, pp. 6932–6944, Nov. 2020.
- [16] Z. Zhang and L. Dai, “A joint precoding framework for wideband reconfigurable intelligent surface-aided cell-free network,” *arXiv preprint arXiv:2002.03744*, Feb. 2020.
- [17] M. Najafi, V. Jamali, R. Schober, and H. Vincent Poor, “Physics-based modeling and scalable optimization of large intelligent reflecting surfaces,” *IEEE Trans. Commun.*, Dec. 2020.
- [18] H. Yang, F. Yang, X. Cao, S. Xu, J. Gao, X. Chen, M. Li, and T. Li, “A 1600-element dual-frequency electronically reconfigurable reflectarray at x/ku-band,” *IEEE Trans. Antennas Propag.*, vol. 65, no. 6, pp. 3024–3032, Jun. 2017.
- [19] D. Headland, T. Niu, E. Carrasco, D. Abbott, S. Sriram, M. Bhaskaran, C. Fumeaux, and W. Withayachumnankul, “Terahertz reflectarrays and nonuniform metasurfaces,” *IEEE J. Sel. Topics Quantum Electron.*, vol. 23, no. 4, pp. 1–18, Aug. 2017.
- [20] C. Hu and L. Dai, “Two-timescale channel estimation for reconfigurable intelligent surface aided wireless communications,” *arXiv preprint arXiv:1912.07990*, Dec. 2019.
- [21] C. Pan, H. Ren, K. Wang, W. Xu, M. ElKashlan, A. Nallanathan, and L. Hanzo, “Multicell MIMO communications relying on intelligent reflecting surfaces,” *IEEE Trans. Wireless Commun.*, vol. 19, no. 8, pp. 5218–5233, Aug. 2020.
- [22] J. Loncar, Z. Sipuš, and S. Hrabar, “Ultrathin active polarization-selective metasurface at X-band frequencies,” *Physical Review B*, vol. 100, no. 7, p. 075131, Oct. 2019.
- [23] J. Bousquet, S. Magierowski, and G. G. Messier, “A 4-GHz active scatterer in 130-nm CMOS for phase sweep amplify-and-forward,” *IEEE Trans. Circuits Syst. I*, vol. 59, no. 3, pp. 529–540, Mar. 2012.
- [24] K. K. Kishor and S. V. Hum, “An amplifying reconfigurable reflectarray antenna,” *IEEE Trans. Antennas Propag.*, vol. 60, no. 1, pp. 197–205, Jan. 2012.
- [25] R. Schroeder, J. He, and M. Juntti, “Passive RIS vs. hybrid RIS: A comparative study on channel estimation,” *arXiv preprint arXiv:2010.06981*, Oct. 2020.
- [26] N. T. Nguyen, Q.-D. Vu, K. Lee, and M. Juntti, “Hybrid relay-reflecting intelligent surface-assisted wireless communication,” *arXiv preprint arXiv:2103.03900*, Mar. 2021.
- [27] K. Ntontin, J. Song, and M. D. Renzo, “Multi-antenna relaying and reconfigurable intelligent surfaces: End-to-end snr and achievable rate,” *arXiv preprint arXiv:1908.07967*, Aug. 2019.
- [28] X. Qian, M. Di Renzo, J. Liu, A. Kammoun, and M. S. Alouini, “Beamforming through reconfigurable intelligent surfaces in single-user MIMO systems: SNR distribution and scaling laws in the presence of channel fading and phase noise,” *IEEE Wireless Commun. Lett.*, vol. 10, no. 1, pp. 77–81, Jan. 2021.
- [29] K. Shen and W. Yu, “Fractional programming for communication systems—part I: Power control and beamforming,” *IEEE Trans. Signal Process.*, vol. 66, no. 10, pp. 2616–2630, May 2018.
- [30] S. Boyd, N. Parikh, E. Chu, B. Peleato, and J. Eckstein, “Distributed optimization and statistical learning via the alternating direction method of multipliers,” Nov. 2014, [Online] Available: https://stanford.edu/~boyd/papers/pdf/admm_distr_stats.pdf.
- [31] X. Chen and F. Yang, “Nonlinear electromagnetic surfaces: Theory, design and application,” [Online] Available: <http://etds.lib.tsinghua.edu.cn/Thesis/>, Master Thesis in Tsinghua University, May 2020.